Available online at www.sciencedirect.com
SCIENCE DIRECT
Polymer 46 (2005) 7456–7462
polymer
www.elsevier.com/locate/polymer

ABA triblock copolymer-based model networks in the bulk: Effect of the number of arms on microphase behavior

Marcin Karbarz[a,b], Zbigniew Stojek[b], Costas S. Patrickios[a,*]

[a]*Department of Chemistry, University of Cyprus, 75 Kallipoleos St, P.O. Box 20537, Nicosia 1678, Cyprus*
[b]*Department of Chemistry, Warsaw University, Pasteura 1, PL-02-093 Warsaw, Poland*

Received 7 May 2005; received in revised form 8 June 2005; accepted 12 June 2005
Available online 7 July 2005

Abstract

The microphase separation behavior in the strong segregation limit of model networks based on cross-linked ABA triblock copolymers in the bulk was investigated by calculating analytically the Gibbs free energies of the various possible morphologies: The spherical, the cylindrical, the lamellar, the reverse cylindrical, the reverse spherical and the disordered. In addition to the elastic and interfacial components, a free energy expression describing the interaction between the network junctions was also introduced. Free energy minimization allowed the construction of a phase diagram with axes the junction functionality and the composition. The phase diagram shows that an increase in the junction functionality leads to an expansion of the region of spheres at the expense of cylinders, and to an eventual elimination of reverse spheres in favor of reverse cylinders. The domain sizes for each morphology were also calculated analytically.

Keywords: Thermodynamic model; Microphase separation; Model polymer networks

1. Introduction

Amphiphilic networks [1] represent a relatively new class of polymeric materials, comprising cross-linked polymers with both hydrophilic and hydrophobic segments, which, similar to their linear counterparts, microphase separate in water [2–4]. The presence of water, as the solvent, and the sometimes charged nature of these polymer networks complicate their thermodynamic description [5,6]. With the aim of understanding the microphase separation behavior of cross-linked polymers, the simplest possible cross-linked polymer system, that comprising nonionic, cross-linked polymers in the absence of any solvent, is investigated here analytically. This polymer system was assumed to be a model network, comprising end-linked ABA triblock copolymers of well-defined length and composition, as well as a precisely defined number of arms at the junction. The present approach is based on analytical expressions for the free energies of microphase-separated linear block copolymers in the bulk in the strong segregation limit [7], complemented by free energy terms describing the interaction among different neighboring junctions [8]. The main result of this study is a morphological phase diagram with independent variables the number of arms and the polymer composition.

2. Theory

We consider a model polymer network [9] with the following attributes: Precise chain lengths between cross-links, elastic chains based on ABA triblock copolymers (the junctions are at the ends of the A-blocks), the ends of each elastic chain connected only to adjacent cross-links (no elastic chain with both ends connected to the same cross-link), constant functionality of the cross-link, and no entanglements. The model network system can exist either in a disordered (D) state or in an ordered state. Five ordered morphologies were considered: The spherical (S), the cylindrical (C), the lamellar (L), the reverse cylindrical

* Corresponding author. Tel.: +35 722 892 768; fax: +35 722 892 801.
E-mail addresses: karbarz@ucy.ac.cy (M. Karbarz), karbarz@chem.uw.edu.pl (M. Karbarz), stojek@chem.uw.edu.pl (Z. Stojek), costasp@ucy.ac.cy (C.S. Patrickios).

0032-3861/$ - see front matter © 2005 Elsevier Ltd. All rights reserved.
doi:10.1016/j.polymer.2005.06.021

(rC) and the reverse spherical (rS). The unit cells for the different morphologies are depicted within Fig. 2 below. Each unit cell contains one cross-link at its center and it comprises one half of each arm (number of arms$=f$) emanating from the cross-link. In each unit cell the conformations of three polymer chains are indicated, each toward one of the three Cartesian co-ordinates. However, in the subsequent calculations the number of arms per cross-link will be varied systematically.

The total free energy for the ordered microphases is given as the sum of four terms: The elastic free energies of the two microphases $\Delta G^{A}_{elastic}$ and $\Delta G^{B}_{elastic}$, the interfacial free energy $\Delta G_{interfacial}$, and the junction–junction interaction free energy $\Delta G_{interaction}$:

$$\Delta G^{ordered}_{total} = \Delta G^{A}_{elastic} + \Delta G^{B}_{elastic} + \Delta G_{interfacial} + \Delta G_{interaction} \quad (1)$$

Microphase A is always the one comprising the black chains with the polymer junctions, and this phase is indicated in gray in the schematic representations of Fig. 2. Microphase B is the one in white, comprising the mid-blocks of the chains.

The total free energy for the disordered case is given by the enthalpic component of the free energy of mixing:

$$\Delta G^{disordered}_{total} = \Delta H_{mixing} = f k_B T \chi N \phi_A (1 - \phi_A) \quad (2)$$

where k_B is Boltzmann's constant, T is the absolute temperature, χ is Flory–Huggins interaction parameter between segments A and B, N is the total number of statistical segments per arm in the unit cell (equal to one half of the total number of statistical segments of the elastic chain), and ϕ_A is the volume fraction of the monomer units of type A.

Assuming Gaussian chains, the elastic free energies $\Delta G^{A}_{elastic}$ and $\Delta G^{B}_{elastic}$ are given by:

$$\Delta G^{A}_{elastic} = \alpha^{A} f k_B T \left(\frac{R}{aN^{1/2}}\right)^2 \quad (3)$$

and

$$\Delta G^{B}_{elastic} = \alpha^{B} f k_B T \left(\frac{R}{aN^{1/2}}\right)^2 \quad (4)$$

where R is a measure of the domain size, a is the statistical segment length, and α^{A} and α^{B} are coefficients that depend on the composition ϕ_A and the morphology. The α^{A} and α^{B} coefficients were approximated with those for linear block copolymers [7], whose expressions are given in Table 1.

The interfacial free energy $\Delta G_{interfacial}$ was calculated from [7]:

$$\Delta G_{interfacial} = \beta f k_B T \frac{aN}{R} \left(\frac{\chi}{6}\right)^{1/2} \quad (5)$$

where β is another coefficient, whose expressions are also given in Table 1.

The junction–junction interaction free energy $\Delta G_{interfacial}$ was estimated from a modified expression originally developed by Semenov [8] to describe micelle–micelle interaction and subsequently used by Hadziioannou and co-workers [10] to describe star–star interaction:

$$\Delta G_{interaction} = k_B T \frac{(f-2)^2}{16\pi} \frac{a}{d} \quad (6)$$

where d is the distance between the interacting junctions, and is related to R via volume balance. The expressions for d for the different morphologies are given in Table 2, and their derivation is provided in the Appendix. The table contains no expression for d for normal spheres because it was considered that no junction–junction interaction takes place in this morphology. This is justified by the fact that the junctions are located within the A spheres which are 'insulated' from each other by the matrix phase B. For reverse cylinders, there are two expressions for d because there are two types of interactions (occurring at two different distances). One type involves three neighbors on the same level, and the other type involves two neighbors, one above and the other below the junction under consideration. Table 2 also shows the corresponding expressions for the free energies of interaction for the different morphologies.

The total free energies of the five morphologies were minimized analytically with respect to the only independent variable, R. With the exception of lamellae, the total free energies of all other morphologies contained R in powers of $+2$ and -1 only, readily leading to expressions for R at the free energy minimum in the form of cube roots. In the case of lamellae, the free energy components contained R in powers of $+2$, -1 and $+0.5$. In this case, the polynomial equation obtained after setting the free energy derivative equal to zero was transformed to a quadratic, which was easily solved.

3. Results and discussion

Table 3 lists the results for R and $\Delta G^{ordered}_{total}$ at the free energy minimum of each morphology. Fig. 1 plots the minimum free energies for the five morphologies plus the disordered state as a function of ϕ_A for three different values of f, 2 (linear multi-block copolymer), 20 and 200. The value of 200 can be realized in some network systems [11–13], whose cross-links are created by the repeated addition of divinyl cross-linkers [14,15]. The values for parameters χ and N, necessary for the calculations, were chosen to be 0.2 and 500, respectively. As the value of f increases, the value of the minimum free energy for the L, C, rC and rS morphologies increases due to an increase in the junction–junction interaction free energy component per chain. The prevailing morphology for given values of ϕ_A and f is that with the lowest minimum free energy. The dominant

Table 1
Expressions for the coefficients for the elastic free energies and the interfacial energy for the various morphologies

Morphology	α^A	α^B	β
Lamellar	$(\pi^2/8)(\phi_A)$	$(\pi^2/8)(1-\phi_A)$	1
Cylindrical	$(\pi^2/16)$	$\frac{\pi^2}{16}\frac{(1-\phi_A^{1/2})^3(3+\phi_A^{1/2})}{(1-\phi_A)^2}$	$2\phi_A^{1/2}$
Reverse cylindrical	$\frac{\pi^2}{16}\frac{\left[1-(1-\phi_A)^{1/2}\right]^3\left[3+(1-\phi_A)^{1/2}\right]}{\phi_A^2}$	$(\pi^2/16)$	$2(1-\phi_A)^{1/2}$
Spherical	$\frac{3\pi^2}{80}\frac{1}{\phi_A^{1/3}}$	$\frac{3\pi^2}{80}\frac{(1-\phi_A^{1/3})^3(6+3\phi_A^{1/3}+\phi_A^{2/3})}{(1-\phi_A)^2}$	$3\phi_A^{2/3}$
Reverse spherical	$\frac{3\pi^2}{80}\frac{\left[1-(1-\phi_A)^{1/3}\right]^3\left[6+3(1-\phi_A)^{1/3}+(1-\phi_A)^{2/3}\right]}{\phi_A^2}$	$(3\pi^2/80)(1/(1-\phi_A))^{1/3}$	$3(1-\phi_A)^{2/3}$

contributions to the minimum free energy were from the elastic and interfacial components, with the junction–junction interaction component contributing one order of magnitude less.

The prevailing morphologies are mapped in Fig. 2 in the form of a phase diagram with axes ϕ_A and f. Schematic representations of these morphologies are provided in the same figure, in which the inter-junction distances d are also defined. The values chosen for parameters χ and N were the same as those used in Fig. 1. Going from left to right, the following microphases are encountered: D–S–C–L–rC–rS–D, as is the case with the phase diagram of linear diblocks [7]. However, compared to linear block copolymers, there is a significant influence of the number of arms on the phase behavior. At low values of ϕ_A, as the number of arms increases, the normal spherical phase increases at the expense of the normal cylindrical phase. This is due to the energetically unfavorable junction–junction interactions, which increase with the number of arms in the case of the cylindrical morphology. In contrast, due to the isolation of the spherical domains containing the junctions, no junction–junction interaction was included in the calculations in the case of the spherical morphology, as explained above.

At high ϕ_A values, as the junction functionality increases, the boundary between reverse spheres and reverse cylinders is slightly shifted initially in favor of the former and later in favor of the latter. At an f value of approximately 150, the reverse spherical morphology disappears completely, while the reverse cylindrical morphology grows correspondingly, indicating that the junction–junction interactions are weaker in the case of the reverse cylindrical morphology compared to the reverse spherical.

Our results are qualitatively similar to those of Matsen and Schick [16] on a related branched segmented copolymer system: Starblock copolymers. These workers investigated theoretically the effect of the number of arms of star copolymers on their morphology in the bulk, and they found that as the number of arms increased from 2 to 9, the region of normal spheres expanded while that of reverse spheres contracted. This similarity in the phase behavior is not surprising because the model polymer networks of the present investigation can be considered as covalently interconnected starblock copolymers.

Theoretical work on the modeling of the morphology of polymer networks is scarce. Existing work [17] involves Monte Carlo simulations on AB diblock copolymers in the bulk, which are randomly cross-linked, resulting in networks, which are not model (not well-defined). The effective functionality at the branching point is low (equal to 3) and the observed morphologies are similar to those of the noncross-linked system: Lamellae for balanced compositions and cylinders or spheres for asymmetrical compositions. However, these morphologies are distorted due to the cross-linking imperfections. Similarly irregular microphases were also observed from Monte Carlo simulations of randomly cross-linked bicomponent homopolymer blends [18].

Finally, we make a comparison between the predictions of our model and some experimental results. The available experimental results are not on model networks but on segmented networks (not ideal structure). Moreover, these experimental studies did not involve a systematic investigation of the number of arms of the junctions, which was in most cases 3. Thus, what these experiments indicate is that cross-linked systems behave

Table 2
Expressions for the junction–junction distances and for the corresponding interaction free energies for the various morphologies

Morphology	d	$\Delta G_{interaction}/fk_BT$
Lamellar	$(fNa^3/2R)^{1/2}$	$\frac{\sqrt{2}}{4\pi}\frac{(f-2)^2}{f^{3/2}}\frac{R^{1/2}}{a^{1/2}N^{1/2}}=\gamma\frac{R^{1/2}}{a^{1/2}}$
Cylindrical	$(fNa^3/\pi R^2)$	$\frac{1}{8}\frac{(f-2)^2}{f^2}\frac{R^2}{a^2N}=\gamma\frac{R^2}{a^2}$
Reverse cylindrical	$(2/\pi)(fNa^3/R^2)$, $(2\pi/3^{3/2})^{1/2}R$	$\frac{1}{16}\frac{(f-2)^2}{f^2}\frac{R^2}{a^2N}+\frac{3^{7/4}}{2^{9/2}\pi^{3/2}}\frac{(f-2)^2}{f}\frac{a}{R}=\gamma_1\frac{R^2}{a^2}+\gamma_2 aR^{-1}$
Spherical	–	–
Reverse spherical	$(4\pi/3)^{1/3}R$	$\frac{3^{4/3}}{2^{11/3}\pi^{4/3}}\frac{(f-2)^2}{f}\frac{a}{R}=\gamma aR^{-1}$

Table 3
Expressions for the minimum free energies and the corresponding domain sizes for the various morphologies

Morphology	$\Delta G_{\text{total}}^{\min}/fk_{\text{B}}T$	$R^{\min}/a$
Lamellar	$((\alpha^{\text{A}}+\alpha^{\text{B}})/N)(R^{\min}/a)^2+\gamma(R^{\min}/a)^{1/2}+\beta' N(R^{\min}/a)^{-1}$	$\left(\frac{-0.5\gamma+\sqrt{0.25\gamma^2+8\beta'(\alpha^A+\alpha^B)}}{4N^{-1}(\alpha^A+\alpha^B)}\right)^{2/3}$
Cylindrical	$(3/2^{2/3})N^{1/3}\beta'^{2/3}(\alpha^A+\alpha^B+N\gamma)^{1/3}$	$(\beta' N^2/2(\alpha^A+\alpha^B+N\gamma))^{1/3}$
Reverse cylindrical	$(3/2^{2/3})N^{1/3}(\gamma_2+N\beta')^{2/3}(\alpha^A+\alpha^B+N\gamma_1)^{1/3}$	$((\gamma_2+\beta' N)N/2(\alpha^A+\alpha^B+N\gamma_1))^{1/3}$
Spherical	$(3/2^{2/3})N^{1/3}\beta'^{2/3}(\alpha^A+\alpha^B)^{1/3}$	$(\beta' N^2/2(\alpha^A+\alpha^B))^{1/3}$
Reverse speherical	$(3/2^{2/3})N^{-1/3}(\gamma+N\beta')^{2/3}(\alpha^A+\alpha^B)^{1/3}$	$[(\gamma+\beta' N)N/2(\alpha^A+\alpha^B)]^{1/3}$

$\beta'=\beta(\chi/6)^{1/2}$

rather similarly to noncross-linked block copolymers, a finding of our theoretical predictions as well.

The experimental results are as follows. In three instances [19–21], bicomponent networks with polyisobutylene (PIB) macro-cross-linker compositions from 49 to 64% w/w, i.e. balanced compositions, yielded lamellar morphologies, consistent with Fig. 2 for $f=3$. In particular, a poly(ethyl acrylate)-PIB (PEA-PIB) network with 49% w/w PIB was characterized by small-angle neutron scattering (SANS) and was determined to form a lamellar morphology [19]. Two poly(2-hydroxyethyl methacrylate)-PIB (PHEMA-PIB) networks with 64% [20] and 57% [21] w/w PIB were determined to form also lamellar morphologies, using, in these cases, small-angle X-ray scattering (SAXS) for characterization. Another experimental system which marginally failed to conform with the predictions of Fig. 2 concerns a network based on a polybutadiene-*b*-polydiethylsiloxane-*b*-polybutadiene (PB-*b*-PDES-*b*-PB) triblock copolymer with 67% w/w PB, cross-linked randomly at the PB end-blocks [22]. This network formed reverse (PDES) cylinders, whereas Fig. 2 would predict lamellae for this composition and for any number of arms; a PB volume fraction above 70% would be required by Fig. 2 for the reverse cylindrical morphology to form. Lastly, a PHEMA-PIB network with 24% w/w PIB macro-cross-linker exhibited a spherical morphology [21], whereas Fig. 2 predicts normal cylinders for this composition and for $f=3$. The discrepancy can be attributed either to an underestimation of the junction–junction interaction by our model or to a higher than three effective number of arms in the experimental system.

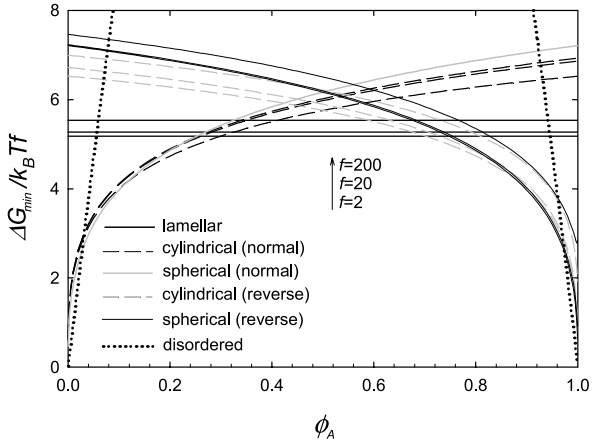

Fig. 1. Dependence of the total free energy minimum of the various morphologies on polymer composition ϕ_{A} and for three different values of the junction functionality.

It is noteworthy that characterization by atomic force microscopy (AFM) of some of the above networks in the bulk almost always revealed sponge-like (spheroidal) morphologies for compositions 23–69% w/w of the macro-cross-linker phase [4,20]. This could be due to the relatively low MWs of the macro-cross-linker chains in these networks (1000–5000 g mol^{-1}), which would lead to small domain sizes, near the resolution limit of AFM.

4. Conclusions

The microphase separation behavior in the strong segregation limit of model networks based on end-linked ABA triblock copolymers was investigated using analytical equations for the free energy. The total free energy comprised three types of components: Elastic, interfacial and junction–junction interaction, the last describing the extra deformation arising from the proximity of two branched (star) structures. The total free energy was minimized analytically to obtain the composition- and functionality- (number of arms-) dependence of the domain size and morphology. It was determined that at large functionalities the regions of spherical and reverse spherical morphology expand and contract, respectively, relative to those of the corresponding cylindrical morphologies. Systematic and carefully-conducted characterization (preferably by SAXS and SANS) studies on well-defined polymer networks are necessary to thoroughly test the predictions of the model.

Acknowledgements

The European Commission is thanked for providing a Marie Curie grant (HPMT-CT-2001-00421) that enabled the stay of MK at the University of Cyprus.

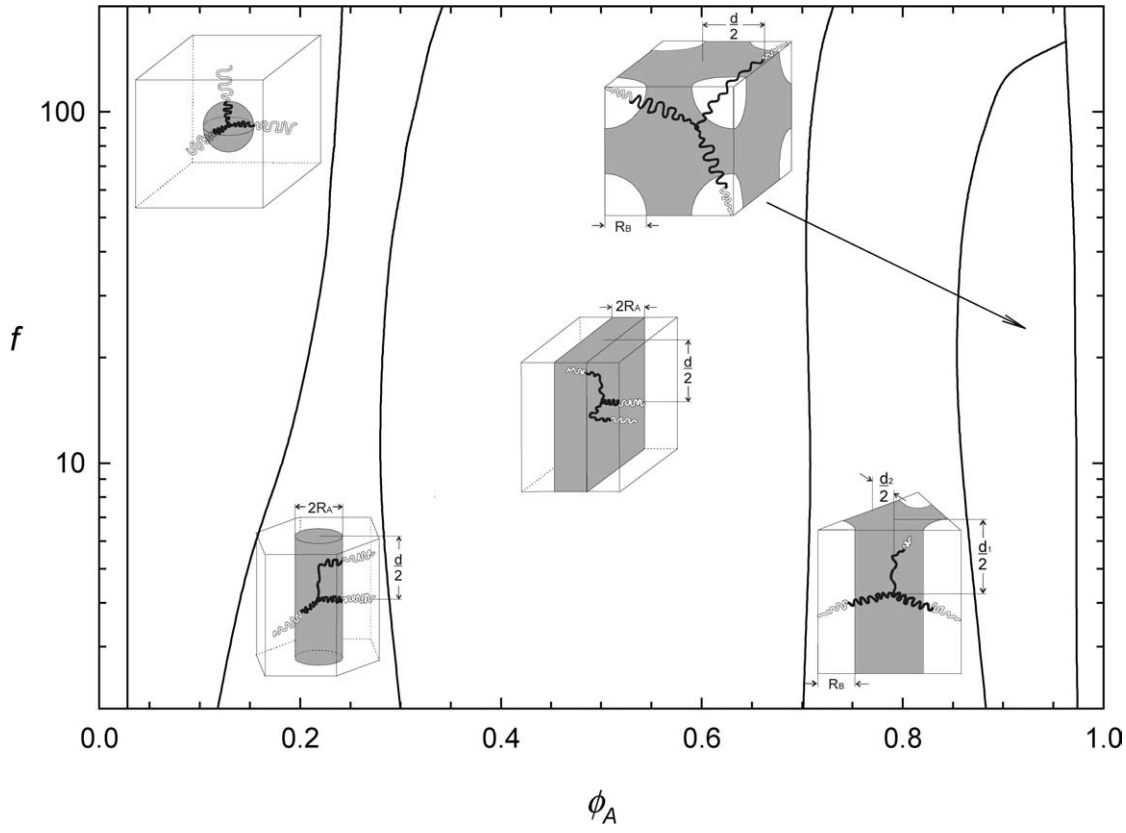

Fig. 2. Phase diagram for ABA triblock copolymer-based model networks as a function of polymer composition ϕ_A and the number of arms at the junction.

Appendix

We provide below the calculations of the distances d between the junctions for the various morphologies in which there are junction–junction interactions. Distances d are indicated in the schematic representations of the morphologies illustrated in Fig. 2.

Lamellar morphology

Volume balance (polymer incompressibility) in the lamellar microphase A dictates:

$$(2R_A)d^2 = fN\phi_A a^3 \tag{A1}$$

where $2R_A$ is the thickness of domain A, illustrated schematically in Fig. 2. R_A is related to R via:

$$R_A = R\phi_A \tag{A2}$$

Using Eq. (A2) to eliminate R_A in Eq. (A1) and solving for d leads to the expression for d for lamellae provided in Table 2.

Cylindrical morphology

Similarly, volume balance in the cylindrical core (microphase A) dictates:

$$(\pi R_A^2)d = fN\phi_A a^3 \tag{A3}$$

where R_A here is the radius of the cylinder, illustrated schematically in Fig. 2. R_A is related to R by:

$$R_A = R\phi_A^{1/2} \tag{A4}$$

Using Eq. (A4) to eliminate R_A in Eq. (A3) and solving for d leads to the expression for d for cylinders provided in Table 2.

Reverse cylindrical morphology

There are two characteristic distances, d_1 and d_2, for this morphology. The calculations here would not involve only the cylindrical core (microphase B), as was the case for normal cylinders, but the whole unit cell, which is a triangle parallelepiped, illustrated in Fig. 2. The size of domain B (radius of B cylinders) R_B and the distances d_1 and d_2 are all illustrated in Fig. 2. R_B is related to R via the volume fraction of B, ϕ_B:

$$R_B = R\phi_B^{1/2} \tag{A5}$$

If x is the side of the triangle, the cross-sectional area A of

the triangle would be:

$$A = \frac{\sqrt{3}}{4}x^2 \tag{A6}$$

The cross-sectional area of microphase B on that triangle is that of three one-sixth cylinders:

$$A_{\text{cylinder}} = \frac{3}{6}\pi R_{\text{B}}^2 = \frac{\pi}{2}R_{\text{B}}^2 \tag{A7}$$

A_{cylinder} and A are interrelated through ϕ_{B} as follows:

$$\phi_{\text{B}} = \frac{A_{\text{cylinder}}}{A} = \frac{2\pi}{\sqrt{3}}\frac{R_{\text{B}}^2}{x^2} \tag{A8}$$

The last expression can be easily solved for x:

$$x = \left(\frac{2\pi}{\phi_{\text{B}}\sqrt{3}}\right)^{1/2} R_{\text{B}} \tag{A9}$$

which can be combined with Eq. (A5) to give:

$$x = \left(\frac{2\pi}{\sqrt{3}}\right)^{1/2} R \tag{A10}$$

Substituting x from Eq. (A10) into Eq. (A6) yields:

$$A = \frac{\pi}{2}R^2 \tag{A11}$$

Volume balance in the unit cell yields:

$$Ad_1 = fNa^3 \tag{A12}$$

where d_1 is the distance between consecutive junctions along the axis vertical to the plane of the triangle. Solving for d_1 in Eq. (A12) and using Eq. (A11) leads to:

$$d_1 = \frac{2}{\pi}\frac{fNa^3}{R^2} \tag{A13}$$

already listed in Table 2.

The distance d_2 between adjacent junctions lying on the same plane (vertical to the axis of the cylinder) is given by simple geometry:

$$d_2 = \frac{2}{3}h \tag{A14}$$

where h is the height of the triangle, related, via trigonometry, to x by:

$$h = \frac{\sqrt{3}}{2}x \tag{A15}$$

Combining Eq. (A14) with Eq. (A15), d_2 becomes:

$$d_2 = \frac{\sqrt{3}}{3}x \tag{A16}$$

which, using the expression for x in Eq. (A10), becomes:

$$d_2 = \left(\frac{2\pi}{3^{3/2}}\right)^{1/2} R \tag{A17}$$

also listed in Table 2.

Reverse spherical morphology

The characteristic distance d for the reverse spherical morphology is that between the centers of two adjacent cubes (unit cells), at which the junctions are located. This distance as well as the size of domain B (radius of B spheres) R_{B} are illustrated in Fig. 2. Thus, the side of the cube is equal to d. R_{B} is related to R via the volume fraction of B, ϕ_{B}:

$$R_{\text{B}} = R\phi_{\text{B}}^{1/3} \tag{A18}$$

The volume of microphase B in the unit cell is that of eight spherical octants of a B sphere:

$$V_{\text{sphere}} = \frac{8}{8}\frac{4\pi}{3}R_{\text{B}}^3 = \frac{4\pi}{3}R_{\text{B}}^3 \tag{A19}$$

Using Eq. (A18) to eliminate R_{B} from Eq. (A19) yields:

$$V_{\text{sphere}} = \frac{4\pi}{3}\phi_{\text{B}}R^3 \tag{A20}$$

On the other hand, ϕ_{B} is the ratio of the volume of microphase B, V_{sphere}, divided by the total volume of the unit cell, d^3:

$$\phi_{\text{B}} = \frac{V_{\text{sphere}}}{d^3} = \frac{4\pi}{3}\phi_{\text{B}}\frac{R^3}{d^3} \tag{A21}$$

Solving for d yields:

$$d = \left(\frac{4\pi}{3}\right)^{1/3} R \tag{A22}$$

already listed in Table 2.

References

[1] Patrickios CS, Georgiou TK. Curr Opin Colloid Interf Sci 2003;8:76–85.
[2] Park D, Keszler B, Galiatsatos V, Kennedy JP. J Appl Polym Sci 1997;66:901–10.
[3] Bruns N, Tiller JC. Nano Lett 2005;5:45–8.
[4] Bruns N, Scherble J, Hartmann L, Thomann R, Iván B, Mülhaupt R, et al. Macromolecules 2005;38:2431–8.
[5] Vamvakaki M, Patrickios CS. J Phys Chem B 2001;105:4979–86.
[6] Georgiou TK, Vamvakaki M, Patrickios CS. Polymer 2004;45:7341–55.
[7] Matsen MW, Bates FS. J Chem Phys 1997;106:2436–48.
[8] Semenov AN. Sov Phys JETP 1985;61:733–42.
[9] Hild G. Prog Polym Sci 1998;23:1019–149.
[10] Grayer V, Dormidontova EE, Hadziioannou G, Tsitsilianis C. Macromolecules 2000;33:6330–9.
[11] Simmons MR, Yamasaki EN, Patrickios CS. Macromolecules 2000;33:3176–9.
[12] Triftaridou AI, Hadjiyannakou SC, Vamvakaki M, Patrickios CS. Macromolecules 2002;35:2506–13.
[13] Vamvakaki M, Patrickios CS. Chem Mater 2002;14:1630–8.
[14] Simms JA, Spinelli HJ. J Coat Technol 1987;59:125–31.
[15] Simms JA. Rubber Chem Technol 1991;64:139–51.
[16] Matsen MW, Schick M. Macromolecules 1994;27:6761–7.
[17] Uchida N. J Phys: Condens Matter 2004;16:L21–L7.

[18] Lay S, Sommer J-U, Blumen A. J Chem Phys 2000;113:11355–63.
[19] Iván B, Almdal K, Mortensen K, Johannsen I, Kops J. Macromolecules 2001;34:1579–85.
[20] Scherble J, Thomann R, Iván B, Mülhaupt R, Tiller JC. J Polym Sci, Part B: Polym Phys 2001;39:1429–36.
[21] Domján A, Erdödi G, Wilhelm M, Neidhöfer M, Landfester K, Iván B, et al. Macromolecules 2003;36:9107–14.
[22] Molenberg A, Möller M, von Soden W. Acta Polym 1998;49:45–51.